Histochem Cell Biol (2010) 134:23–30
DOI 10.1007/s00418-010-0706-x

ORIGINAL PAPER

Combined immunoelectron microscopic and computer-assisted image analyses to detect advanced glycation end-products in human myocardium

Cameron Donaldson · Douglas J. Taatjes · Michael Zile · Bradley Palmer · Peter VanBuren · Francis Spinale · David Maughan · Michele Von Turkovich · Nicole Bishop · Martin M. LeWinter

Accepted: 4 May 2010 / Published online: 19 May 2010

Abstract Advanced glycation end-products (AGEs) result from oxidation–reduction reactions that ensue when a sugar becomes adducted to a protein. AGEs cause various complications of diabetes mellitus (DM). Experimental and clinical evidence suggest that AGEs also contribute to the complications of hypertension (HTN). Little is known about the abundance and localization of AGEs in *human* myocardium. In a few light microscopic studies, the AGE carboxymethyl lysine (CML) has been immunolabeled and localized virtually exclusively to the walls of small arteries. To more precisely delineate the abundance and localization of CML, we developed an immunoelectron microscopic (IEM) detection method using anti-CML monoclonal antibody 6D12 in conjunction with computer-assisted image analysis. Antibody was pre-absorbed with purified AGE-bovine serum albumin to assure specificity. Antigen–antibody (ag–ab) complexes were individually identified with protein A-conjugated colloidal gold and counted with an automated system. We applied this method in 21 patients (pts) undergoing epicardial biopsy during coronary bypass grafting (CBG) [20 M, 1 F; mean age 65 ± 7.4 (± SEM) years]. Seven pts had neither DM nor HTN, seven had HTN, and seven had DM + HTN. In contrast to the prior light microscopic studies, we detected CML scattered throughout the cardiomyocyte in all pts, but in widely varying amounts. Ag–ab complexes were abundant in sections through myofilaments (mean count 23.6 ± 9.2 per μm^2, range 9.4–48) and even more so in mitochondria (mean count 34.4 ± 11.9 per μm^2, range 14.1–68.2, $P < 0.001$ vs. myofilaments). CML was also detected in vascular endothelial cells. There were no statistically significant differences based on presence or absence of HTN or DM. In conclusion, our IEM method is the first to provide detailed delineation of the localization and abundance of CML in myocardium. CML is very prevalent in CBG pts, suggesting that AGEs could play a role in abnormal cardiomyocyte function, including altered energy metabolism.

Keywords Immunoelectron microscopy · Advanced glycation end-products · Diabetes mellitus · Myocardium

C. Donaldson (✉) · D. J. Taatjes · B. Palmer · P. VanBuren · D. Maughan · M. Von Turkovich · N. Bishop · M. M. LeWinter
Department of Physiology and Biophysics, University of Vermont School of Medicine, 145 Beaumont Ave, Burlington, VT 05405, USA
e-mail: cameron.donaldson@uvm.edu

M. Zile · F. Spinale
RHJ Department of Veterans Affairs Medical Center, Medical University of South Carolina, Charleston, SC 29425, USA

Introduction

Advanced glycation end-products (AGEs) are formed via non-enzymatic oxidation–reduction reactions in which glucose first becomes adducted to a protein and is then converted into a series of carbonyl intermediates via the Maillard reaction (Thormally 2005; Wautier and Schmidt 2004). AGEs can form on many proteins, including collagen, hemoglobin, and myocardial contractile and calcium cycling proteins (Aronson 2003; Cooper 2004; Li et al. 2005; Tan et al. 2002; Yoshida et al. 2005; Zieman et al. 2005). Certain AGEs can also form cross-links between adjacent protein molecules (Avery and Bailey 2006).

AGEs and associated cross-links can produce an array of functional modifications linked to changes in protein charge, hydrophilicity, elasticity, and turnover. Thus,

enzyme activity can be altered, lipoproteins may not be recognized by the low-density lipoprotein (LDL) receptor with resulting impaired clearance from the blood, and cross-linking can stiffen collagen as well as make it more resistant to the effects of matrix metalloproteinases (Ohno et al. 2006; Witztum et al. 1982).

In addition to these direct effects, the receptor for AGEs (RAGE) activates a MAP kinase signaling pathway resulting in induction of activated cytokines and the nuclear transcription factor κB (NF κB) (Yeh et al. 2001). The downstream effects of this pathway include changes in matrix metalloproteinases, tissue inhibitors of matrix metalloproteinases, and TGFβ that increase collagen content and tissue stiffness (Candido et al. 2003; Kim et al. 2005; Naka et al. 2004; Simm et al. 2004; Yan et al. 2003).

Increased AGEs have been recognized for many years as an important mechanism leading or contributing to various complications of diabetes mellitus (DM). AGEs have been detected in myocardium in animals with experimental DM and are thought to contribute to the various manifestations of DM that comprise diabetic cardiomyopathy (Berg et al. 1999; Schafer et al. 2006). These include abnormalities of ion pumps and contractile proteins, abnormal energy metabolism and increased passive stiffness due to the aforementioned effects on collagen (van Heerebeek et al. 2008).

In addition to DM, AGEs may play a role in the pathophysiology of other disease processes. This is suggested by the results of several clinical trials employing the AGE cross-link breaker ALT-711 (Alagebrium). In a clinical trial conducted in elderly women with isolated systolic hypertension (HTN) due to reduced arterial compliance, administration of ALT-711 resulted in normalization of arterial compliance and lowering of systolic blood pressure (Kass et al. 2001). In another study in patients (pts) with isolated systolic HTN, ALT-711 improved endothelial function (Zieman et al. 2007). In a small trial in pts with heart failure and preserved left ventricular (LV) ejection fraction (EF), ALT-711 resulted in normalization of echocardiographic indexes of diastolic function (Little et al. 2005). AGEs also appear to play a role in the progression of atheroma, perhaps via RAGE activation and promotion of the generation of reactive oxygen species (Chen et al. 2010).

There is virtually no information about the abundance and distribution of AGEs in human myocardium. Three previous studies using light microscopic immunolocalization of the AGE carboxymethyl lysine (CML), two in postmortem specimens and one in LV endomyocardial biopsy material from pts with heart failure, have identified AGEs in small arteries in pts with and without DM, with virtually no localization elsewhere (Nakamura et al. 1993; van Heerebeek et al. 2008; Yoshida et al. 1998). These results are in agreement with a recent light microscopic immunolocalization study in elderly hypertensive canines demonstrating that CML is confined to the vasculature and occurs in the myocardium only in association with arterioles (Shapiro et al. 2008). These studies suggest that AGEs do not have an important role in cardiomyocyte or extracellular matrix abnormalities.

We hypothesized that a method providing improved resolution and sensitivity for detection of AGEs would allow a more complete understanding of their distribution within the myocardium. Accordingly, we developed a combined colloidal gold immunoelectron microscopic (IEM)/stereologic method to localize and quantify CML in LV myocardial tissue obtained by biopsy at the time of coronary bypass surgery. We report details of the method here and a preliminary assessment of quantification and localization.

Materials and methods

Patient selection and clinical characteristics

Twenty-one pts (20 males and 1 female) undergoing coronary bypass graft (CBG) surgery were recruited. Their mean age was 64 $\pm$ 7.4 ($\pm$ SE) years. All had normal preoperative LV EF and contraction pattern assessed by echocardiography and/or left ventriculography. None had a history of acute myocardial infarction. Seven pts had a history of both HTN and DM, seven had a history of HTN alone, and seven did not have a history of either HTN or DM. The diagnosis of HTN in each case was based on a history of elevated blood pressure and treatment with antihypertensive drugs. Each of the pts with DM had a HgbA1c determination performed in close proximity to their CBG surgery. All pts gave informed consent for intra-operative myocardial biopsy and signed a consent document approved by the University of Vermont Committee on Research in Human Subjects.

Specimen preparation for immunoelectron microscopy

Epicardial myocardial biopsies ($\sim$1–2 $\times$ 1 $\times$ 5–8 mm and $\sim$20–50 mg in weight) were obtained from the LV anterior free wall at a site near its minor axis while the pts were on cardiopulmonary bypass, as previously described (Fukagawa et al. 2005). The entire biopsy was immediately placed in a protective solution of Kreb–Ringers solution containing 30 mM 2,3-butanedione monoxime. Soon thereafter an $\sim$1 mm wide specimen was cut from one end of the biopsy with scissors and placed in a solution of fixative consisting of 3% (para)formaldehyde and 0.1% glutaraldehyde in 0.01 M phosphate buffer, 0.15 M NaCl

(PBS). The cut specimens were then fixed for a total of 2 h at 4°C. After rinsing with PBS, free aldehyde groups were quenched by rinsing two times for 30 min in 0.05 M NH_4Cl in PBS. After rinsing again with PBS, the tissue was dehydrated in ethanol at progressively lower temperatures and infiltrated and embedded in the hydrophilic resin Lowicryl K4M (Carlemalm et al. 1982; Roth et al. 1981).

Immunoelectron microscopy

Antigenic sites for the AGE, Clone No. 6D12, were labeled using the post-embedding pAg technique, as previously described (Fanburg et al. 1997; Mount et al. 1993a, b, 1995a, b, 1996; Mount and Taatjes 1994; Roth et al. 1978; Taatjes et al. 1993, 1994; Valente et al. 1995). Ultrathin sections (60–80 nm thick) were cut with a diamond knife and placed onto formvar/carbon-coated 200 mesh nickel grids (Ladd Research, Williston, VT, USA). The grids were floated, section side down, for 20 min on drops of 0.5% ovalbumin in PBS, followed by incubation on drops of diluted mouse monoclonal anti-AGE antibody [Cosmo Bio USA Inc., Carlsbad, CA, USA; 2.5 μg/ml in PBS/1.0% bovine serum albumin (BSA)] for 18 h at 4°C. After three rinses of 5 min each with PBS/BSA, the grids were floated on drops of affinity purified rabbit anti-mouse IgG (10 μg/ml; Jackson ImmunoResearch Laboratories, West Grove, PA, USA) for 30 min at room temperature. After three rinses of 5 min each with PBS/BSA, the grids were incubated on drops of protein A/gold, 10 nm size particles (pAg10; prepared in our lab), for 1 h at room temperature. The pAg10 was diluted with PBS containing 1% BSA, 0.075% Triton-X100, and 0.075% Tween 20 to give an optical density of 0.06 at 525 nm. After rinsing with PBS/BSA and then distilled water, grids were contrasted with 3% aqueous uranyl acetate and lead citrate, and examined in a JEOL 1210 transmission electron microscope (JEOL Ltd USA, Peabody, MA, USA) operating at 60 kV. Negative controls for the immunocytochemical procedures included sections incubated with rabbit anti-mouse IgG followed by pAg and sections incubated with pAg alone. Pre-absorption controls for antibody specificity are described in detail below.

Pre-absorption of anti-AGE antibody with purified antigen

Extensive characterization of the clone 6D12 mouse monoclonal antibody by Ikeda et al. (1996) indicate that the antibody binds to an epitope consisting of a CML-protein adduct. In their manuscript, Ikeda et al. (1996) showed that clone 6D12 monoclonal antibody strongly binds to purified AGE-BSA samples. Thus, to demonstrate the specificity of our immunostaining technique for AGE-protein adducts in the tissue specimens, we pre-absorbed the antibody with purified AGE-BSA (Fitzgerald Industries International, Concord, MA, USA), and used this preparation for incubation with the sections. Briefly, 10 μl volumes of various concentrations of AGE-BSA were added to a 10-μl volume of a 5-μg/ml anti-AGE monoclonal antibody to yield final concentrations of 500, 250, 125, 50, 25, 12.5, and 5 μg/ml AGE-BSA in 2.5 μg/ml of antibody. The antigen–antibody (ag–ab) mixture was vortexed and allowed to stand for 60 min at room temperature, followed by incubation on grids as described earlier.

Transmission electron microscopic imaging by systematic random sampling

Each specimen removed from the biopsy yielded one to five blocks of tissue. Thick sections (1 μm thick) from each block were prepared with glass knives and stained with 1% toluidine blue. Following viewing of the sections by light microscopy, one block from each biopsy was chosen based upon the greatest amount of longitudinally sectioned myofibrils present, and then thin sectioned. The thin sections were retrieved onto grids, and then each grid was visually inspected with a dissecting microscope. One grid was chosen from each group of grids based upon showing a centrally located and intact section (without tears or wrinkles) and immunolabeled with the anti-AGE monoclonal antibody. For each labeled thin section, a grid square was chosen from the corner of the section and one field containing mostly myofibrils and one field containing mostly mitochondria were photographed at 30,000× microscope magnification. The specimen grid was moved horizontally so that two subsequent grid squares were skipped, and the third grid square was used to photograph the next fields of myofibrils and mitochondria. This routine was continued horizontally and then vertically, sampling every third grid square until 25 fields of myofibrils and 25 fields of mitochondria were photographed. Images were captured on Kodak 4489 electron microscope film, and the negatives were scanned on a digital scanner (ScanMaker 8700, Microtek International Inc.) to obtain digital images displaying a resolution of 600 dpi.

Anti-AGE quantification of myofibrils

Computer-assisted image analysis was performed to quantitate the number of colloidal gold particles (indicative of anti-AGE binding sites) over myofibrils from the various pt biopsies. Scanned images were opened in MetaMorph image analysis program (Universal Imaging Corp., West Chester, PA, USA). After calibrating distances (based upon a scale bar included on each negative), a standardized region of interest rectangle representing approximately

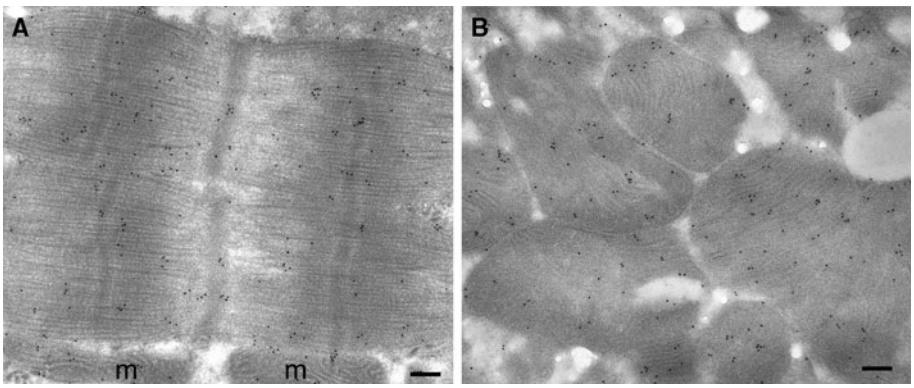

Fig. 1 Immunoelectron microscopic detection of anti-CML binding sites on ultrathin sections of Lowicryl K4M-embedded human myocardium biopsies. Colloidal gold particles are distributed throughout the myofibrils (**a**) and mitochondria (**b**). *m* Mitochondrion. *Bars* 200 nm

3 μm^2 was placed over a centralized area on the image containing only myofibrils. A color threshold was applied to the gold particles and thresholded areas representing individual gold particles were automatically counted and logged to an Excel spreadsheet. The quantity of gold particles was expressed as the number per μm^2 of myofibril. This procedure was repeated for each of the 25 images of myofibrils for each biopsy.

Anti-AGE quantification of mitochondria

As described earlier for myofibrils, images were opened in MetaMorph image analysis program. After calibrating distances, the stylus tool was used to trace a region around the perimeter of mitochondria identified within the myofibril areas. The area of each mitochondrion was measured and logged to an Excel spreadsheet. Subsequently, a color threshold was applied to include only the gold particles, and thresholded areas representing individual gold particles were automatically counted and logged to an Excel spreadsheet. The quantity of gold particles was expressed as the number per μm^2 of mitochondrium.

Data analysis and statistics

All grouped data are expressed as mean ± SEM. Patients were divided into three groups consisting of those with neither HTN nor DM, HTN only, and HTN + DM ($n = 7$ in each group). CML counts were compared amongst the three groups using repeated measures ANOVA. CML counts in myofibril fields and mitochondria were compared using a paired t test with a correction for multiple comparisons.

Results

Colloidal gold particles indicative of anti-AGE binding sites were identified in all of the biopsies and were found to be widely distributed within cardiomyocytes, but preferentially in myofibril sections and within mitochondria (Fig. 1). This immunostaining was abolished by pre-absorbing the antibody with purified AGE-BSA prior to incubation with the sections (Fig. 2). Stereological protocols were developed to quantitate the number of colloidal gold particles (indicative of anti-CML binding sites) associated with myofibrils and mitochondria. Figure 3 illustrates the cellular areas chosen for quantification outlined in red, while the colloidal gold particles thresholded and automatically counted within these areas are depicted in yellow. For all of the biopsies, counts in fields including myofibrils averaged 23.6 ± 9.2 per μm^2 (range 9.4–48.0). Mitochondrial counts were 34.4 ± 11.9 per μm^2 (range 14.1–68.2), significantly greater than the myofibril counts ($P < 0.001$). Collagen fibrils, however, were very sparsely labeled, if at all (Fig. 3). Small blood vessels were occasionally encountered in the biopsy specimens and showed immunostaining over endothelial cells and red blood cells (Fig. 4). Immunostaining associated with blood vessels and red blood cells was inhibited by pre-absorption of the anti-CML antibody with AGE-BSA adducts (not shown). Nuclei of both cardiomyocytes and endothelial cells consistently demonstrated weak but positive immunostaining (Figs. 2, 5).

In the group without HTN or DM, myofibril counts were 22.7 ± 8.1 per μm^2 and mitochondrial counts were 31.5 ± 10.6 per μm^2. In the HTN group these values were 22.1 ± 11 and 34.5 ± 15.3 per μm^2, respectively, while in the HTN + DM group they were 25.2 ± 8.1 and 36.2 ± 8.3 per μm^2, respectively. The difference between myofibril and mitochondrial counts was significant in each group ($P < 0.0001$), but there were no significant differences between groups based on the presence or absence of HTN or DM. HgbA1c ranged from 5.5 to 8.6 in the seven pts with DM. There was no significant correlation between HgbA1c and either myofibril or mitochondrial CML counts. Finally, there was no significant correlation of CML counts with age of the pts.

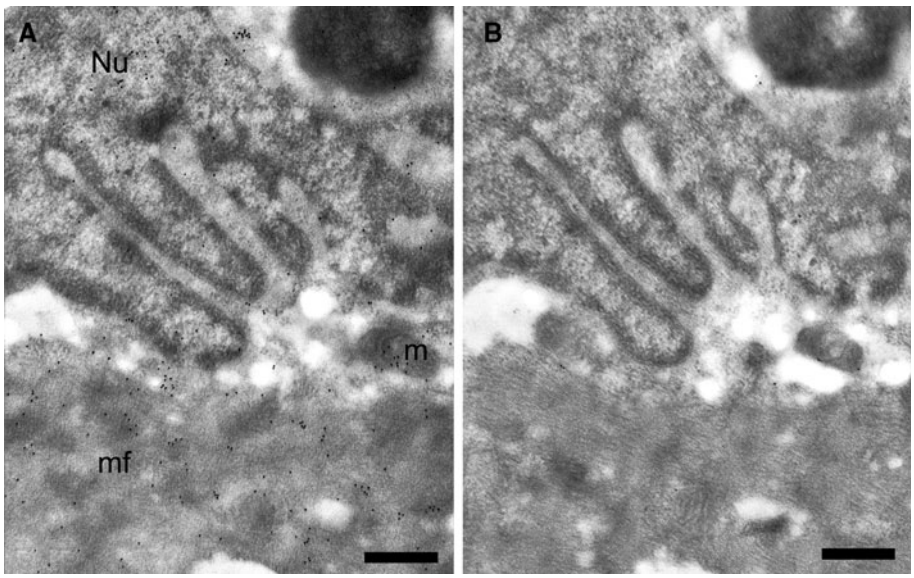

Fig. 2 Demonstration of antibody pre-absorption control indicating specificity of anti-CML clone 6D12 antibody for CML-protein adduct. Serial (not consecutive) ultrathin sections were incubated either with the anti-CML antibody alone followed by protein A-gold (**a**), or with the anti-CML antibody preabsorbed with AGE-BSA adduct, followed by protien A-gold (**b**). Note that the immunostaining present over the myofibrils (*mf*), mitochondrion (*m*), and nucleus (*Nu*) in (**a**) is essentially eliminated by pre-absorption of the antibody with AGE-BSA (**b**). *Scale bars* 500 nm

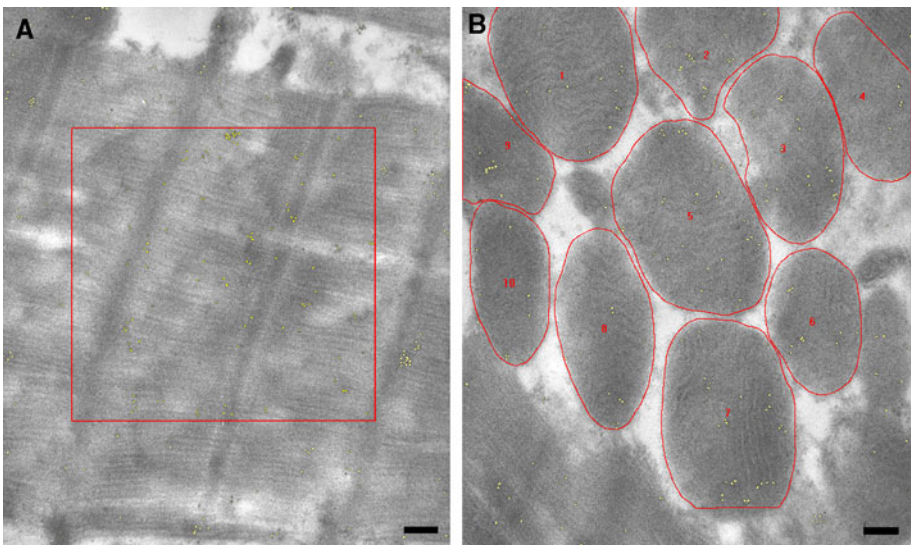

Fig. 3 Demonstration of computer-assisted image analysis for quantitating anti-CML binding sites over myofibrils and mitochondria from ultrathin sections of human cardiac muscle. **a** The region of interest over myofibrils is delineated by a *red box*, while the colloidal gold particles counted are *pseudocolored yellow*. **b** Individual mitochondria were manually outlined in *red* (with a number associated with each traced region), and the colloidal gold particles counted within the traced regions *pseudocolored yellow*. *Scale bars* 200 nm

Discussion

The IEM method we developed to detect the AGE CML reveals that the epitope is widely distributed throughout the cardiomyocyte in pts undergoing CBG surgery. CML was detectable in all pts, but in widely varying amounts. CML is a particularly significant AGE because it appears to be important in AGE–RAGE interaction. Of note, CML was present in systematically greater amounts in mitochondria than in sections through myofibrils, suggesting the potential for involvement of AGEs in disordered energy metabolism. This may also suggest that AGEs tend to form preferentially in portions of the cell that are most susceptible to oxidative stress. We also detected CML in cardiomyocyte nuclei. Since there are numerous other AGEs, it is reasonable to assume that the overall AGE abundance is much greater than what we observed for CML alone. There was no obvious pattern to the distribution of CML in myofibril sections or within mitochondria and therefore we cannot speculate which proteins or other molecules they are associated with.

In addition to cardiomyocytes, CML was also detectable in endothelial cells in small arteries, including their nuclei. However, we did not detect appreciable CML in association with collagen fibrils in any of the groups. In DM in particular, AGEs play a major role in stiffening of collagen in other tissues, e.g., skin (Meerwaldt et al. 2007). We speculate that our inability to detect significant amounts of collagen-associated CML is because of the fact that CML is an AGE that does not significantly cross-link (Smit and

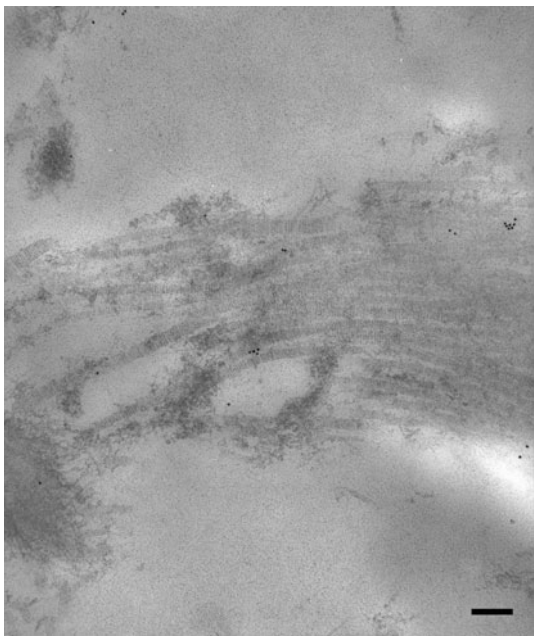

Fig. 4 Ultrathin section from Lowicryl K4M-embedded human myocardium shows only negligible immunostaining with anti-CML antibody present over collagen fibrils. *Scale bar* 200 nm

Lutgers 2004). As discussed earlier, AGE cross-links are particularly prevalent in collagen. They are also long-lasting and their presence might tend to limit adduction of other, non-cross-linking AGEs to a given protein. There are numerous AGEs, and details regarding which cross-link and to what extent they do so have not been fully elucidated. In the future, it will be of great interest to repeat these studies using an AGE such as pentosidine, which is known to extensively cross-link (Ulrich and Cerami 2001).

Our results contrast with previous human studies examining CML localization with immunohistochemistry by light microscopy. As noted earlier, in the latter studies CML was detected virtually exclusively in small arteries, with little or no localization at other sites. A major advantage of our method compared with light microscopy is that the use of colloidal gold allows identification of individual ag–ab complexes as well as precise quantitation of their abundance. Light microscopic methods likely allow AGE detection most easily in areas where ag–ab complexes are in very close proximity or clustered together, as opposed to the scattered distribution we observed using IEM. As an added control for the specificity of this very well-characterized monoclonal antibody, we pre-absorbed the antibody with specific antigen (AGE-BSA) prior to immunolabeling. The resulting attenuation of gold particle staining provides further support that the immunostaining present in cardiomyocytes results from the presence of immunodetectable CML.

Our finding that CML was detected in all pts, regardless of whether DM or HTN was present, suggests that AGE formation is very common. However, the presence of coronary artery disease in our pts, which is often associated with increased oxidative stress, makes it impossible for us to reach any firm conclusions about AGE formation in normal subjects. At the same time, our pts had normal LV contraction patterns, which should minimize coexistent ischemic myocardial damage and, therefore, associated oxidative stress. Although we found no correlation between pt age and AGE counts, the presence of AGEs in much older pts with systolic HTN due to reduced arterial compliance (Kass et al. 2001), a condition that exaggerates the normal aging process, supports the idea that AGEs may become more abundant simply with aging.

The fact that we did not detect any significant differences in CML abundance amongst the three groups of pts, including those with DM, is perhaps not surprising considering the relatively small size of each group and the

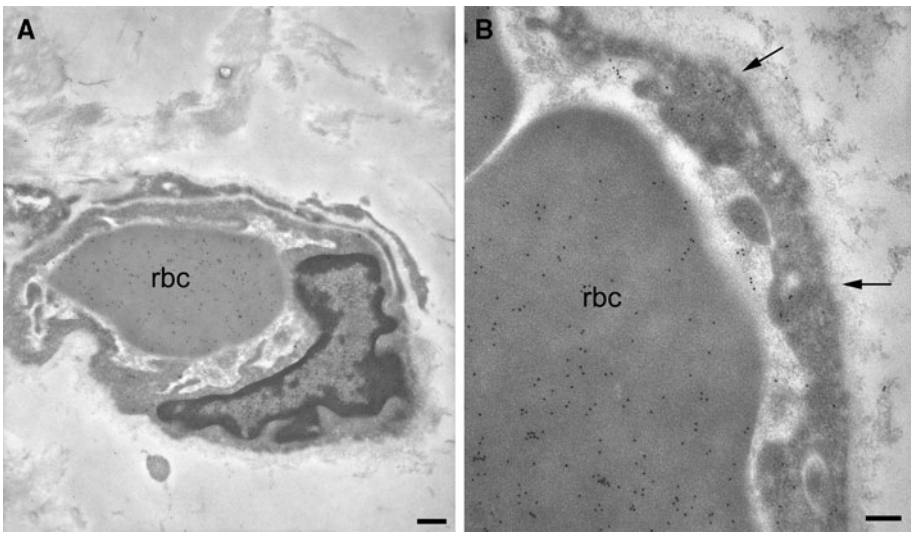

Fig. 5 Ultrathin sections from Lowicryl K4M-embedded human myocardium demonstrating immunostaining with anti-CML antibody over blood vessel components. **a** Low magnification image shows staining over endothelial cell cytoplasm and nucleus, as well as over red blood cells (*rbc*). **b** At higher magnification, the immunostaining of the endothelial cell (*arrows*) and red blood cell (*rbc*) in vessel lumen is apparent. *Scale bars* 500 nm (**a**); 200 nm (**b**)

potential for individual variations in AGE abundance. Biopsies were not taken from multiple sites, though a systematic effort was made to obtain tissue at a consistent location, hopefully minimizing differences due to regional variation. Other major potential sources of such variation include the duration and severity of HTN, DM, and associated coronary artery disease and differences in the treatment of these conditions. Lack of a correlation between HgbA1c and CML counts in the pts with DM is also not surprising given their relatively small number and the fact that most HgbA1c values fell in a narrow range. Finally, it is possible that other AGEs are distributed differently than CML and would have demonstrated significant variations between the diagnostic groups. We suspect that detection of differences in myocardial AGE abundance based on the presence or absence of DM or HTN, if they exist, will require larger numbers of pts.

In summary, our IEM method revealed extensive accumulation of CML throughout cardiomyocytes in pts with coronary artery disease undergoing CBG, with even greater accumulation within mitochondria. CML was also detected in vascular endothelial cells. There was minimal accumulation of this AGE in association with collagen fibrils. The wide distribution of CML suggests that AGEs could contribute to a variety of cardiomyocyte abnormalities, including abnormal calcium handling, contractile protein alterations and deranged energy metabolism. Additional studies will be required to gain a better understanding of the determinants of AGE abundance and their functional significance.

Acknowledgments This research was supported by NIH grants RO1 HL089944 and T32 HL07647. We thank Drs. John Ikonomidis, Frank Ittleman, Bruce Leavitt, Mitchell Norotsky, Joseph Schmoker and John Toole, who performed the intra-operative biopsies.

References

Aronson D (2003) Cross-linking of glycated collagen in the pathogenesis of arterial and myocardial stiffening of aging and diabetes. J Hypertens 21:3–12

Avery NC, Bailey AJ (2006) The effects of the Maillard reaction on the physical properties and cell interactions of collagen. Pathol Biol 54(7):387–395

Berg TJ, Snorgaard O, Faber J, Torjesen PA, Hildebrandt P, Mehlsen J, Hanssen KF (1999) Serum levels of advanced glycation end products are associated with left ventricular diastolic function in patients with type 1 diabetes. Diabetes Care 22:1186–1190

Candido R, Forbes JM, Thomas MC, Thallas V, Dean RG, Burns WC, Tikellis C, Ritchie RH, Twigg SM, Cooper ME, Burrell LM (2003) A breaker of advanced glycation end products attenuates diabetes-induced myocardial structural changes. Circ Res 92(7):785–792

Carlemalm E, Garavito RM, Villiger W (1982) Resin development for electron microscopy and an analysis of embedding at low temperature. J Microsc 126:123–143

Chen J, Song M, Yu S, Gao P, Yu Y, Wang H, Huang L (2010) Advanced glycation endproducts alter functions and promote apoptosis in endothelial progenitor cells through receptor for advanced glycation endproducts mediate overpression of cell oxidant stress. Mol Cell Biochem 335(1–2):137–146

Cooper ME (2004) Importance of advanced glycation end products in diabetes-associated cardiovascular and renal disease. Am J Hypertens 17:31S–38S

Fanburg JC, Rosenberg AE, Weaver DL, Leslie KO, Mann KG, Taatjes DJ, Tracy RP (1997) Osteocalcin and osteonectin immunoreactivity in the diagnosis of osteosarcoma. Am J Clin Pathol 107:464–473

Fukagawa NK, Palmer BM, Barnes WD, Leavitt BJ, Ittleman FP, Lewinter MM, Maughan DW (2005) Acto-myosin crossbridge kinetics in humans with coronary artery disease: influence of sex and diabetes mellitus. J Mol Cell Cardiol 39(5):743–753

Ikeda K, Higashi T, Sano H, Jinnouchi Y, Yoshida M, Araki T, Ueda S, Horiuchi S (1996) *N* (Carboxymethyl) lysine protein adduct is a major immunological epitope in proteins modified with advanced glycation end products of the Maillard reaction. Biochemistry 35:8075–8083

Kass DA, Shapiro EP, Kawaguchi M, Capriotti AR, Scuteri A, Degroof RC, Lakatta EG (2001) Improved arterial compliance by a novel advanced glycation end-product crosslink breaker. Circulation 104:1464–1470

Kim W, Hudson BJ, Moser B, Guo J, Rong LL, Lu Y, Qu W, Lalla E, Lerner S, Chen Y, Yan SS, D'Agati V, Naka Y, Ramasamy R, Herold K, Yan SF, Schmidt AM (2005) Receptor for advanced glycation end products and its ligands: a journey from the complications of diabetes to its pathogenesis. Ann N Y Acad Sci 1043:553–561

Li SY, Du M, Dolence EK, Fang CX, Mayer GE, Ceylan-Isik AF, LaCour KH, Yang X, Wilbert CJ, Sreejayan N, Ren J (2005) Aging induces cardiac diastolic dysfunction, oxidative stress, accumulation of advanced glycation endproducts and protein modification. Aging Cell 4:57–64

Little WC, Zile MR, Kitzman DW, Hundley WG, O'Brien TX, Degroof RC (2005) The effect of alagebrium chloride (ALT-711), a novel glucose cross-link breaker, in the treatment of elderly patients with diastolic heart failure. J Card Fail 11:191–195

Meerwaldt R, Lutgers HL, Links TP, Graaff R, Baynes JW, Gans RO, Smit AJ (2007) Skin autofluorescence is a strong predictor of cardiac mortality in diabetes. Diabetes Care 30(1):107–112

Mount SL, Taatjes DJ (1994) Neuroendocrine carcinoma of the skin (Merkel cell carcinoma): an immunoelectron microscopic case study. Am J Dermatopathol 16:60–65

Mount SL, Taatjes DJ, Trainer TD (1993a) Ultrastructural study of a pituitary adenoma (prolactinoma) within the clivus bone using immunoelectron microscopy. Ultrastruct Pathol 17:639–664

Mount SL, Taatjes DJ, von Turkovich M, Tindle BH, Trainer TD (1993b) Diagnostic immunoelectron microscopy in surgical pathology: assessment of various tissue fixation and processing protocols. Ultrastruct Pathol 17:547–557

Mount SL, Lee KR, Taatjes DJ (1995a) Carcinosarcoma (malignant mixed mullerian tumor) of the uterus with a rhabdoid tumor component: an immunohistochemical, ultrastructural and immunoelectron microscopic case study. Am J Clin Pathol 103:235–239

Mount SL, Weaver DL, Taatjes DJ, McKinnon WC, Hebert JC (1995b) Von Hippel-Lindau disease presenting as pancreatic neuroendocrine tumor. Virchows Arch A Pathol Anat 426:523–528

Mount SL, Dickerman J, Taatjes DJ (1996) Extrarenal Wilm's tumor: an ultrastructural and immunoelectron microscopic case report. Ultrastruct Pathol 20:155–165

Naka Y, Bucciarelli LG, Wendt T, Lee LK, Rong LL, Ramasamy R, Yan SF, Schmidt AM (2004) RAGE axis: animal models and novel insights into the vascular complications of diabetes. Arterioscler Thromb Vasc Biol 24:1342–1349

Nakamura Y, Horii Y, Nishino T, Shiiki H, Sakaguchi Y, Kagoshima T, Dohi K, Makita Z, Vlassara H, Buccala R (1993) Immunohistochemical localization of advanced glycosylation end products in coronary atheroma and cardiac tissue in diabetes mellitus. Am J Pathol 143:1649–1656

Ohno S, Im HJ, Knudson CB, Knudson W (2006) Hyaluronan oligosaccharides induce matrix metalloproteinase 13 via transcriptional activation of NFkappaB and p38 MAP kinase in articular chondrocytes. J Biol Chem 281:17952–17960

Roth J, Bendayan M, Orci L (1978) Ultrastructural localization of intracellular antigens by the use of protein A-gold complex. J Histochem Cytochem 26:1074–1081

Roth J, Bendayan M, Carlemalm E, Villiger W, Garavito M (1981) Enhancement of structural preservation and immunocytochemical staining in low temperature embedded pancreatic tissue. J Histochem Cytochem 29:663–671

Schafer S, Huber J, Wihler XC, Rutten H, Busch AE, Linz W (2006) Impaired left ventricular relaxation in type 2 diabetic rats is related to myocardial accumulation of *N*(epsilon)-(carboxymethyl) lysine. Eur J Heart Fail 8:206

Shapiro BP, Owan TE, Mohammed SF, Meyer DM, Mills LD, Schalkwijk CG, Redfield MM (2008) Advanced glycation end products accumulate in vascular smooth muscle and modify vascular but not ventricular properties in elderly hypertensive canines. Circulation 118(10):1002–1010

Simm A, Bartling B, Silber RE (2004) RAGE: a new pleiotropic antagonistic gene? Ann N Y Acad Sci 1019:228–231

Smit AJ, Lutgers HL (2004) The clinical relevance of advanced glycation endproducts (AGE) and recent developments in pharmaceutics to reduce AGE accumulation. Curr Med Chem 11:2767–2784

Taatjes DJ, Arendash-Durand B, von Turkovich M, Trainer TD (1993) HMB-45 antibody demonstrates melanosome-specificity by immunoelectron microscopy. Arch Pathol Lab Med 117:264–268

Taatjes DJ, Mount SL, Trainer TD, Tindle BH (1994) Localization of anti Leu-M1 (CD15) binding sites in Hodgkin's disease by immunoelectron microscopic examination. Am J Clin Pathol 101:140–148

Tan KC, Chow WS, Ai VH, Metz C, Bucala R, Lam KS (2002) Advanced glycation end products and endothelial dysfunction in type 2 diabetes. Diabetes Care 25:1055–1059

Thormally PJ (2005) Dicarbonyl intermediates in the Maillard reaction. Ann N Y Acad Sci 1043:111–117

Ulrich P, Cerami A (2001) Protein glycation, diabetes, and aging. Endocr Soc 56:1–21

Valente AM, Taatjes DJ, Mount SL (1995) Comparison of the pattern of expression of Leu-M1 antigen in adenocarcinomas, neutrophils and Hodgkin's disease by immunoelectron microscopy. Histochemistry 103:181–186

van Heerebeek L, Hamdani N, Handoko ML, Falcao-Pires I, Musters RJ, Kupreishvili K, Ijsselmuiden AJ, Schalkwijk CG, Bronzwaer JG, Diamont M, Borbely A, van der Velden J, Stienen GJ, Laarman GJ, Niessen HW, Paulus WJ (2008) Diastolic stiffness of the failing diabetic heart: importance of fibrosis, advanced glycation end products, and myocyte resting tension. Circulation 117:43–51

Wautier JL, Schmidt AM (2004) Protein glycation: a firm link to endothelial cell dysfunction. Circ Res 95:233–249

Witztum JL, Mahoney EM, Branks MJ, Fisher M, Elam R, Steinberg D (1982) Nonenzymatic glucosylation of low-density lipoprotein alters its biologic activity. Diabetes 31(4 Pt 1):283–291

Yan SF, Ramasamy R, Naka Y, Schmidt AM (2003) Glycation, inflammation, and RAGE: a scaffold for the macrovascular complications of diabetes and beyond. Circ Res 93:1159–1169

Yeh CH, Sturgis L, Haidacher J, Zhang XN, Sherwood SJ, Bjercke RJ, Juhasz O, Crow MT, Tilton RG, Denner L (2001) Requirement for p38 and p44/p42 mitogen-activated protein kinases in RAGE-mediated nuclear factor-kappaB transcriptional activation and cytokine secretion. Diabetes 50(6):1495–1504

Yoshida S, Yamada K, Hamaguchi K, Nishimura M, Hatakeyama E, Tsuchida H, Sakamoto K, Kashiwabara H, Yokoyama T, Ikeda K, Horiuchi S (1998) Immunohistochemical study of human advanced glycation end-products (AGE) and growth factors in cardiac tissues of patients on maintenance dialysis and with kidney transplantation. Clin Nephrol 49:273–280

Yoshida N, Okumura K, Aso Y (2005) High serum pentosidine concentrations are associated with increased arterial stiffness and thickness in patients with type 2 diabetes. Metabolism 54:345–350

Zieman SJ, Melenovsky V, Kass DA (2005) Mechanisms, pathophysiology, and therapy of arterial stiffness. Arterioscler Thromb Vasc Biol 25:932–943

Zieman SJ, Melenovsky V, Clattenburg L, Corretti MC, Capriotti A, Gerstenblith G, Kass DA (2007) Advanced glycation endproduct crosslink breaker (alagebrium) improves endothelial function in patients with isolated systolic hypertension. J Hypertens 25(3):577–583